XMS-CASPT2//XMS-CASPT2 and XMS-CASPT2//CASSCF at comparison: The impact of dynamic correlation in the excited state optimization of nitronaphthalene

Angelo Giussani[*,‡] and Javier Segarra-Martí

[‡]Instituto de Ciencia Molecular, Universitat de València, Apartado22085, ES-46071 Valencia, Spain
[*]To whom correspondence should be addressed. Email: Angelo.Giussani@uv.es

Analytic XMS-CASPT2 gradients are here used to rationalize the decreasing triplet quantum yield trend in 2-nitronaphthalene, 1-nitronaphthalene, and 2-methyl-1-nitronaphthalene, a series of nitro-substituted aromatic compounds. Comparison with XMS-CASPT2//CASSCF results highlights the importance of dynamic correlation in geometry optimization and challenge the validity of an XMS-CASPT2//CASSCF approach: XMS-CASPT2 S_1 minima leads to planar structures, while CASSCF optimizations trigger a pyramidalization of the nitro group. XMS-CASPT2 results correlate the reported decreasing triplet quantum yield trend in these species to a decrease in S_1 to T_2 population transfer and an increase of S_1 to S_0 decay, while no such correlation is observed when using XMS-CASPT2//CASSCF data.

The CASPT2//CASSCF approach consists in performing geometrical optimizations at the CASSCF level and refining the energy of the so obtained optimized structures at the CASPT2 level (the // symbol separate the method used for the evaluation of the energy and the method uses for the obtention of the geometries). In such a way the final energies are computed with a method (CASPT2) able to recover both static and dynamic correlation, while the geometrical optimizations are performed with a method (CASSCF) able to describe static but not dynamic correlation. The main assumption of this approach is then that CASSCF and CASPT2 surfaces are practically parallel and have a very similar topology, the only substantial difference a shift in the energies.[4] While the reliability of CASPT2//CASSCF is reflected in its successes over the last 30 years, an actual evaluation of the importance of dynamics correlation for geometrical optimizations has rarely been performed, simply because of the lack of CASPT2 gradients. With the advent of analytical CASPT2 gradients,[1–3] we are now in the position of performing such an important missing test. We here do so study the three nitroaromatic systems 2-nitronaphthalene (2NN), 1-nitronaphthalene (1NN), and 2-methyl-1-nitronaphthalene (2M1NN), which, despite their chemical similarity, present remarkably different triplet quantum yields: 0.93 ± 0.15, 0.64 ± 0.12, and 0.33 ± 0.05, respectively.[5–11]

Nitroaromatics are a vast group of molecules, important in the study of urban air contaminants and energetic materials, and with applications in the drug delivery sector.[12–14] Moreover, nitroaromatics display intrinsically relevant photophysical and photochemical properties, as an unusually, at least for organic molecules, highly efficient decay from the singlet to the triplet manifold. 1NN is in fact considered the organic compound with the fastest multiplicity change ever measured (around 100 fs).[15] The reason behind such an efficient singlet-to-triplet decay is the high spin-orbit coupling characterizing the S_1-$^1(n_A\pi^*)$ and the T_2-$^3(\pi_O\pi^*)$ states (of the order of 60 cm^{-1}) together with the presence of S_1/T_2 intersystem crossing points along the S_1 decay path.[16,17]

Using CASPT2//CASSCF S_1 minima and numerical CASPT2 S_1/S_0 minimum energy conical intersections (MECI), one of us previously justified the reported trend for their triplet quantum yields by the different ability to reach from the former the latter structure, which constitutes a decay path in competition with the population of triplet states.[8] The CASPT2//CASSCF S_1 minima of 2NN, 1NN, and 2M1NN are in fact 0.25, 0.13, and 0.00 eV lower than the corresponding numerical CASPT2 S_1/S_0 MECIs. The higher is this separation, the lower would be the relevance of the S_1-to-S_0 decay, and in turn the higher would be the probability to decay to the triplet manifold. Moreover, at the three

CASPT2//CASSCF S_1 minima, the S_1-$^1(n_A\pi^*)$ and the T_2-$^3(\pi_O\pi^*)$ states are almost degenerate, meaning that at this level of theory for the three molecules the decay to the triplet states is equally probable, so that their different triplet quantum yields should result from a different ability to decay along the competing S_1-to-S_0 path.

Despite that the above described model is consistent with the experimental data, a doubt remains on the influence of using CASSCF S_1 minima, especially because the computation of CASPT2 energies along liner interpolation of internal coordinates (LIIC) paths connecting the minima with the corresponding S_1/S_0 MECIs reveals that the CASSCF minima are not the structures having the lowest CASPT2 energies, since lower CASPT2 energy points (up to 0.29 eV lower) were computed along the LIIC paths.

In the present contribution we recomputed both the S_1 minima and the S_1/S_0 MECIs using CASPT2 analytical gradients, and employing CASPT2 in its extended Multi-State (XMS-CASPT2) version.[18] In order to compare a full XMS-CASPT2 description with a XMS-CASPT2//CASSCF characterization, the S_1 minima and S_1/S_0 MECIs where recomputed also at the latter level of theory.

For the rationalization of the triplet quantum yield of the 2NN, 1NN, and 2M1NN, the following model is assumed. We evaluate the probability of decaying into the triplet manifold through the computation of the energy separation between T_2-$^3(\pi_O\pi^*)$ and S_1-$^1(n_A\pi^*)$ at the latter state minimum (hereafter indicated as $\Delta E(S_1\text{-}T_2)$), and the probability to evolve instead along the competing S_1-to-S_0 non-radiative decay path through the computation of the energy separation between the S_1 minimum and the S_1/S_0 MECI (hereafter indicated as $\Delta E(S_1\text{-}S_1/S_0)$). The smaller is $\Delta E(S_1\text{-}T_2)$ and the larger is $\Delta E(S_1\text{-}S_1/S_0)$, the higher should be the corresponding triplet quantum yield.

XMS-CASPT2 analytical gradients were recently implemented in the OpenMolcas code, here used for all calculations.[19,20] Geometry optimizations, both at the CASSCF and XMS-CASPT2 level, were performed using an active space composed by 14 active electrons distributed in 11 actives orbitals, while for the final evaluation of the energies the space was enlarged up to 18 electrons in 14 orbitals (see Figure S1). Globally, we have then performed calculations at the XMS-CASPT2(18,14)//XMS-CASPT2(14,11) and XMS-CASPT2(18,14)//CASSCF(14,11) level. The CAS(18,14) space includes both the π nature of the system and the lone pairs of the oxygen atoms, while the reduced active space is the result of the exclusion of some orbitals on the basis of their occupation number in the S_0 and S_1 states (see Table S1-S3). Geometry optimizations were performed using the following thresholds for the convergency of the energy and the norm of the gradient: 0.0 and 3.0D-4 au, respectively. The basis set of atomic natural orbitals (ANO) of L-type contracted to C,N,O [3s,2p,1d]/H[2s1p] was employed,[21,22] and all calculations were performed computing state-averaging over two-roots. For the XMS-CASPT2 calculations, an imaginary level-shift correction of 0.2 a.u. was used in order to minimize the effects of possible intruder states, as did in our previous contribution on nitronaphthalene systems.[8] Cholesky decomposition was used to speed up the calculation of two-electron integrals. Numerical frequencies were computed at the obtained CASSCF and XMS-CASPT2 S_1 minima, respectively. Examples of the OpenMolcas inputs employed for CASSCF and XMS-CASPT2 optimizations are reported in Figure S2-S5.

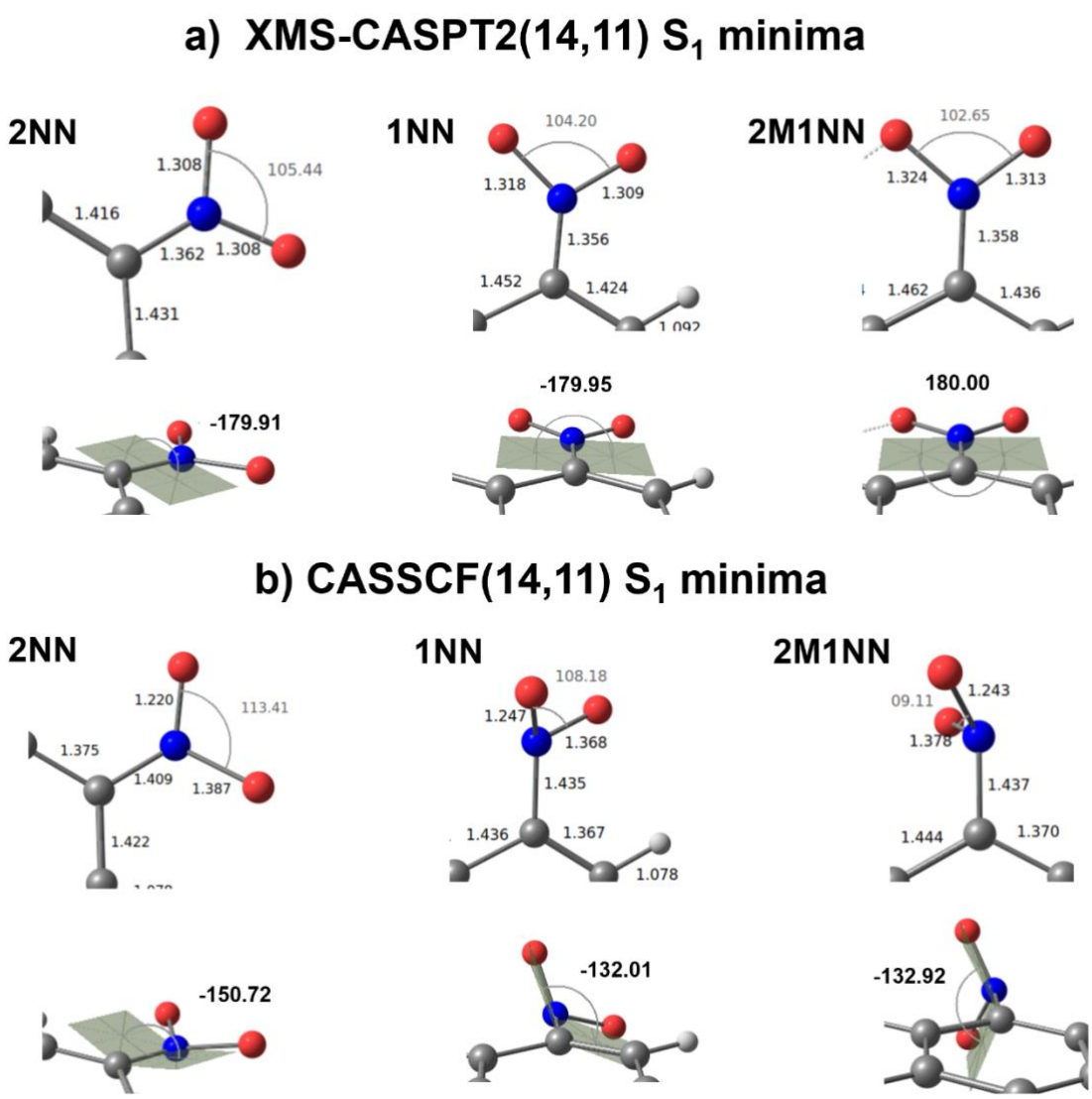

Figure 1. a) nitro group of the S_1 minima, $^1(n_A\pi^*)_{min}$, of 2NN, 1NN, and 2M1NN optimized at the XMS-CASPT2(14,11) level. Selected bond lengths (in Å) and angles (in degrees) are also reported. b) nitro group of the S_1 minima, $^1(n_A\pi^*)_{min}$, of 2NN, 1NN, and 2M1NN optimized at the CASSCF(14,11) level. Selected bond lengths (in Å) and angles (in degrees) are also reported.

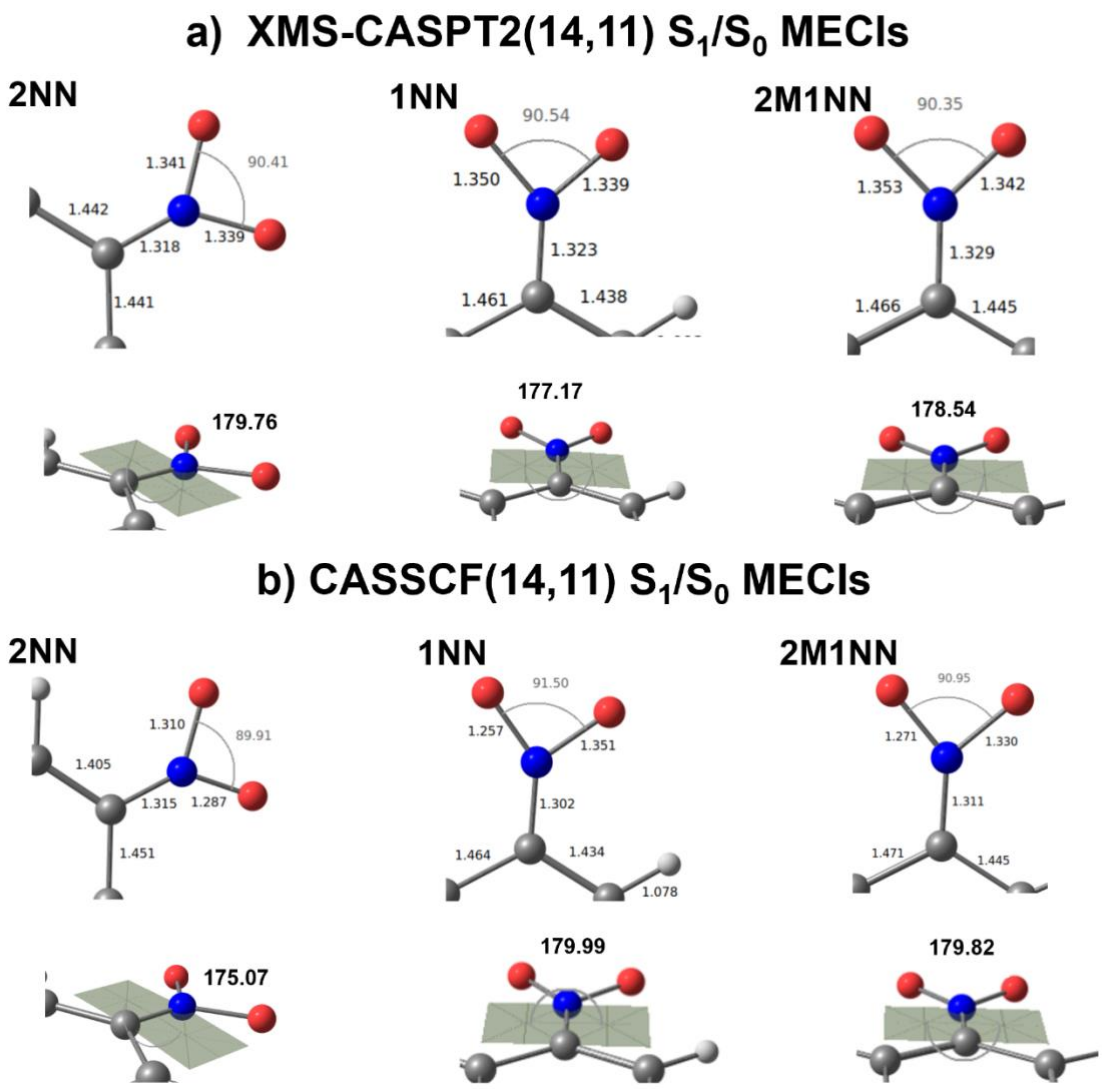

Figure 2. a) nitro group of the S_1/S_0 MECIs, $(^1n_A\pi^*/gs)_{CI}$, of 2NN, 1NN, and 2M1NN optimized at the XMS-CASPT2(14,11) level. Selected bond lengths (in Å) and angles (in degrees) are also reported. b) nitro group of the S_1/S_0 MECIs, $(^1n_A\pi^*/gs)_{CI}$, of 2NN, 1NN, and 2M1NN optimized at the CASSCF(14,11) level. Selected bond lengths (in Å) and angles (in degrees) are also reported.

The geometries of the XMS-CASPT2(14,11) optimized S_1 minima and S_1/S_0 MECIs are reported in Figure S6a and S7a, respectively, while the nitro group of such critical points is displayed in Figure 1a and 2a. The latter figures are focused on the nitro group because is where the main geometrical deformations are localized. The S_1 minima and S_1/S_0 MECIs will be also here indicated as $^1(n_A\pi^*)_{min}$ and $(^1n_A\pi^*/gs)_{CI}$, respectively, since from the analysis of the corresponding wave-functions the S_1 state is indeed the $^1(n_A\pi^*)$ state, following the nomenclature of reference 8 (see Figure S8). The nature of the S_1 equilibrium structure was confirmed computing the corresponding XMS-CASPT2(14,11) numerical frequencies. All optimized geometries are planar structures, expect for the methyl group of the 2M1NN molecule, being the nitro group in the plane of the aromatic rings. For the three systems is possible to appreciate that the same main geometrical deformation characterizes the S_1/S_0 MECIs with respect to the S_1 minima: the C-NO_2 bond distance is significantly reduced, both NO lengths are increased is a symmetric way, and the value of ONO angle decreases. Such a deformation is also observed comparing the S_1 minima with the previously published numerical CASPT2 S_0 minima.[8] This in turn determines that after excitation into the S_1 state, the evolution of the system towards the S_1 minimum is along the same direction that the evolution towards the S_1/S_0 MECI, so that depending

on the relative energies of the two structures, the probability of decaying along the non-radiative decay mediated by the S_1/S_0 MECI will significantly change.

The S_1 structures for the three molecules optimized at the CASSCF(14,11) level of theory starting from the optimized XMS-CASPT2(14,11) geometries are reported in Figure S9. Again the structures appears to be planar, with the nitro group in the plane of the aromatic system. The key difference with respect to the XMS-CASPT2(14,11) minima is that the main deformation displayed by the nitro group is mainly affecting a single NO bond. For example, while at the S_1 minimum of 2NN obtained at the XMS-CASPT2 level the two NO bonds display the same value of 1.308 Å, at the CASSCF structure one NO lengths is equal to 1.226 Å, while the other presents the much larger value of 1.359 Å. The computation of the corresponding CASSCF(14,11) frequencies reveals that these structures are actually not true minima, since in all cases an imaginary frequency (of 153, 65, and 67 cm^{-1} for 2NN, 1NN, and 2M1NN, respectively) which describes the pyramidalization of the nitro group is present. True S_1 CASSCF(14,11) minima were obtained modifying the geometry along the imaginary frequency and re-optimizing. The resulting minima, reported in Figure S6b and 1b, are no longer planar and agreed with the previously published structures obtained at the CASSCF(18,14) level.[8]

Regarding the CASSCF(14,11) S_1/S_0 MECIs (see Figure S7b and 2b), again the main geometrical difference with respect to the XMS-CASPT2(14,11) structures is an asymmetric elongation of the NO bonds. In order to verify the presence of non-planar S_1/S_0 MECIs, the latter were reoptimized starting from the true non-planar S_1 CASSCF minima. Non-planar S_1/S_0 MECIs were obtained, which, being characterized by a significantly higher energy (around 0.7 eV) than the corresponding planar structures, are presumably not photophysically relevant.

Table 1. a) XMS-CASPT2(18,14) energies (eV) of the low-lying singlet and triplet electronic states of 2NN, 1NN, and 2M1NN, computed at the XMS-CASPT2(14,11) optimized critical points.[a] b)XMS-CASPT2(18,14) energies (eV) of the low-lying singlet and triplet electronic states of 2NN, 1NN, and 2M1NN, computed at the CASSCF(14,11) optimized critical points.[a]

a) XMS-CASPT2(18,14)//XMS-CASPT2(14,11)												
	2NN				1NN				2M1NN			
	gs	$^1(n_A\pi^*)$	$^3(\pi_O\pi^*)$	$^3(n_A\pi^*)$	gs	$^1(n_A\pi^*)$	$^3(\pi_O\pi^*)$	$^3(n_A\pi^*)$	gs	$^1(n_A\pi^*)$	$^3(\pi_O\pi^*)$	$^3(n_A\pi^*)$
$^1(n_A\pi^*)_{min}$	-1.71	0.00	0.59	0.02	-1.48	0.00	0.72	0.02	-1.33	0.00	0.88	0.01
$(^1n_A\pi^*/gs)_{CI}$	0.42	0.43	1.77	0.37	0.36	0.35	1.53	0.48	0.30	0.29	1.73	0.24
b) XMS-CASPT2(18,14)//CASSCF(14,11)												
	2NN				1NN				2M1NN			
	gs	$^1(n_A\pi^*)$	$^3(\pi_O\pi^*)$	$^3(n_A\pi^*)$	gs	$^1(n_A\pi^*)$	$^3(\pi_O\pi^*)$	$^3(n_A\pi^*)$	gs	$^1(n_A\pi^*)$	$^3(\pi_O\pi^*)$	$^3(n_A\pi^*)$
$^1(n_A\pi^*)_{min}$	-2.25	0.00	0.07	-0.07	-1.66	0.00	0.22	-0.13	-1.76	0.00	0.19	-0.12
$(^1n_A\pi^*/gs)_{CI}$	0.15	0.09	1.61	0.00	0.00	0.06	1.40	-0.02	0.04	0.08	1.59	-0.01

[a] All the reported values refer to the corresponding $^1(n_A\pi^*)$ state in its minimum.

Table 1a reports the XMS-CASPT2(18,14) low lying singlet and triplet excited states energies at the XMS-CASPT2(14,11) S_1 minima and S_1/S_0 MECIs for the 2NN, 1NN and 2M1NN molecules. It is possible to observe that $\Delta E(S_1\text{-}S_1/S_0)$ is decreasing along the series of molecules, being equal to 0.43, 0.35, and 0.29 eV for 2NN, 1NN, and 2M1NN, respectively. This trend is the same as the one characterizing their triplet quantum yields, consequently supporting the idea that a more accessible S_1/S_0 decay will in turn determine a lower probability of populating the triplet states.
The second key variable that determines the probability of decaying into the triplet manifold is the energy separation between the S_1-$^1(n_A\pi^*)$ and T_2-$^3(\pi_O\pi^*)$ states, which, due to their different nature (see Figure S2), are coupled by a large spin-orbit coupling. $\Delta E(S_1\text{-}T_2)$ appears significantly different

in the three molecules, being equal to 0.59, 0.72, and 0.88 eV, for 2NN, 1NN, and 2M1NN, respectively. These values indicate that along the series of molecules the energy separation between the S_1-T_2 states increases, which can be consequently related with a lower probability of decaying into the triplet manifold and in turn with the decreasing value of the triplet quantum yield along the series.

Table 1b reports the XMS-CASPT2(18,14) low lying singlet and triplet excited states energies at the CASSCF(14,11) S_1 minima and S_1/S_0 MECIs for the 2NN, 1NN and 2M1NN molecules. It is important to notice that recomputing the energies of the CASSCF MECIs at the XMS-CASPT2(18,14) level, the degeneracy between S_1 and S_0 can be considered to be preserved, being their separation at most 0.06 eV. The key difference with respect to the XMS-CASPT2(18,14)//XMS-CASPT2(14,11) results is that now nor $\Delta E(S_1\text{-}S_1/S_0)$ not $\Delta E(S_1\text{-}T_2)$ show any trend along the series. $\Delta E(S_1\text{-}S_1/S_0)$ is very small for the three molecules, being 0.09, 0.06 and 0.08 eV respectively. These low values consequently suggest an efficient S_1-to-S_0 non-radiative decay for the three molecules. Possible barriers along the path connecting the S_1 minima and S_1/S_0 MECIs (indeed displaying significantly different geometries) are here not evaluate according to the adopted model based on adiabatic energy differences. $\Delta E(S_1\text{-}T_2)$ display a similar value of around 0.2 eV for 1NN and 2M1NN, while being 0.1 eV lower for 2NN. These values then do not allow a rationalization of the registered different triplet quantum yields.

A pictorial comparison of the XMS-CASPT2(18,14) energies obtained at the XMS-CASPT2(14,11) and at the CASSCF(14,11) critical points is presented in Figure 3. As expected, at the XMS-CASPT2(18,14) level the energies of the XMS-CASPT2(14,11) optimized points are lower than the corresponding critical points obtained with CASSCF(14,11).

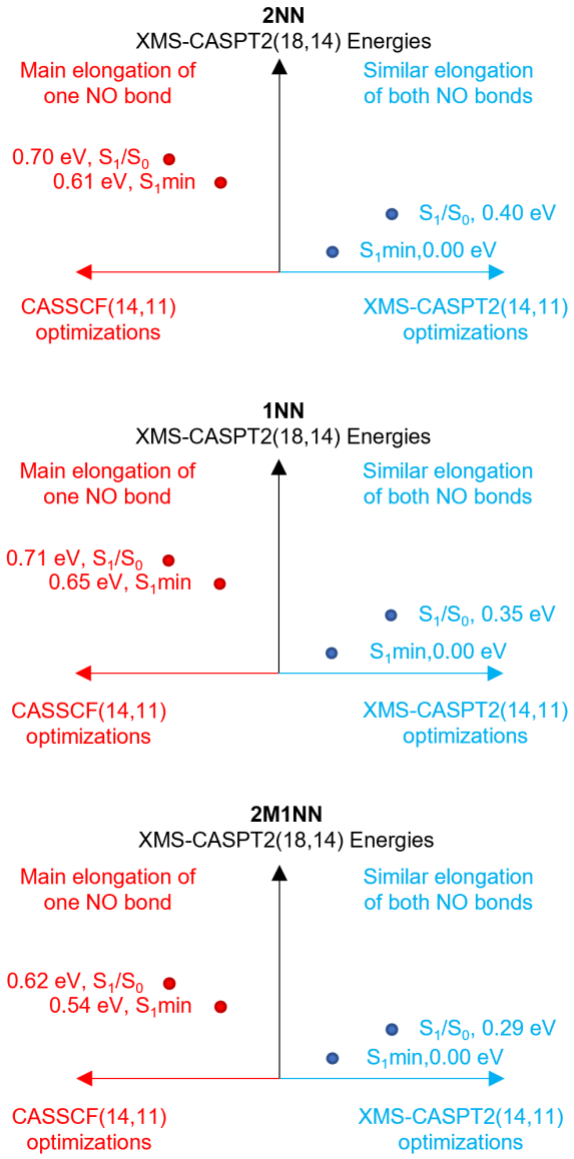

Figure 3. Pictorial representation of the XMS-CASPT2(18,14) energies obtained at the XMS-CASPT2(14,11) and at the CASSCF(14,11) critical points for 2NN, 1NN, and 2M1NN.

As an additional test of the consistency of our model and results, we computed at the XMS-CASPT2(18,14) level the energies along the LIIC paths connecting the XMS-CASPT2(14,11) S_1 minima with the corresponding XMS-CASPT2(14,11) S_1/S_0 MECIs. As shown in Table S4, along these scans the S_1 minima are for the three molecules the lowest points on the S_1 surface, consequently supporting the minimum nature of the optimized S_1 geometries also using the enlarged active space. Moreover, it is not possible to observe any additional barrier along between the two critical points but the one resulting from the adiabatic energy difference, then supporting the use of the latter as a key parameter in our model.

In summary, at the XMS-CASPT2(18,14)//XMS-CASPT2(14,11) level of theory the reasons behind the experimentally measured trend of the triplet quantum yield in the series of molecules 2NN, 1NN, and 2M1NN can be associated to both a reduced ability to decay from the S_1 to the T_2 state and to an increase propensity to evolve in a non-radiative way back to the ground state through the S_1/S_0 MECI. Adopting the same model but working at the XMS-CASPT2(18,14)//CASSCF(14,11) level, it is instead not possible to rationalize their triplet quantum yield, since no significant differences appear among the systems. This consequently illustrate the importance of dynamic correlation in the optimization of critical points, since completely different structures are obtained at the XMS-CASPT2

and CASSCF levels, providing a completely different scenario. This is particularly true for the S_1 minima, where the nitro group is planar and in the plane of the rings at the XMS-CASPT2 points while is pyramidalized according to a CASSCF description. Such a difference can be related to the know tendency of CASSCF to accentuate the single and double bond character and in general to underestimate the degree of conjugation. Also, the here found main geometrical difference between XMS-CASPT2 and CASSCF S_1 minima, is in agreement with the pioneer work of Andruniow and co-workers, comparing numerical CASPT2 and CASSCF S_1 minima for a series of retinal chromophore analogues.[23] In their work, it was also observed that CASSCF fails to locate the planar CASPT2 S_1 minima.

References

1 M. K. MacLeod and T. Shiozaki, Communication: Automatic code generation enables nuclear gradient computations for fully internally contracted multireference theory, *J. Chem. Phys.*, , DOI:10.1063/1.4907717.

2 B. Vlaisavljevich and T. Shiozaki, Nuclear Energy Gradients for Internally Contracted Complete Active Space Second-Order Perturbation Theory: Multistate Extensions, *J. Chem. Theory Comput.*, 2016, **12**, 3781–3787.

3 J. W. Park and T. Shiozaki, On-the-Fly CASPT2 Surface-Hopping Dynamics, *J. Chem. Theory Comput.*, 2017, **13**, 3676–3683.

4 P. Pulay, A Perspective on the CASPT2 Method, *Int. J. Quantum Chem.*, 2011, **111**, 4020–4029.

5 R. A. Vogt and C. E. Crespo-Hernández, Conformational control in the population of the triplet state and photoreactivity of nitronaphthalene derivatives, *J. Phys. Chem. A*, 2013, **117**, 14100–14108.

6 R. A. Vogt, C. Reichardt and C. E. Crespo-Hernández, Excited-state dynamics in nitro-naphthalene derivatives: Intersystem crossing to the triplet manifold in hundreds of femtoseconds, *J. Phys. Chem. A*, 2013, **117**, 6580–6588.

7 C. E Crespo-Hernandez, On the Primary Reaction Pathways in the Photochemistry of Nitro-Polycyclic Aromatic Hydrocarbons, *Mod. Chem. Appl.*, 2013, **01**, 1–7.

8 A. Giussani and G. A. Worth, Similar chemical structures, dissimilar triplet quantum yields: A CASPT2 model rationalizing the trend of triplet quantum yields in nitroaromatic systems, *Phys. Chem. Chem. Phys.*, 2019, **21**, 10514–10522.

9 J. P. Zobel, J. J. Nogueira and L. Gonz, Mechanism of Ultrafast Intersystem Crossing in 2-Nitronaphthalene, *Chem. Eur. J.*, 2018, **24**, 5379–5387.

10 J. P. Zobel, J. J. Nogueira and L. Gonzalez, Finite-temperature Wigner phase-space sampling and temperature effects on the excited-state dynamics of 2-nitronaphthalene, *Phys. Chem. Chem. Phys.*, 2019, **21**, 13906–13915.

11 J. P. Zobel and L. González, Nonadiabatic Dynamics Simulation Predict Intersystem Crossing in Nitroaromatic Molecules on a Picosecond Time Scale, *ChemPhotoChem*, 2019, **3**, 833–845.

12 R. Atkinson, E. C. Tuazon, T. J. Wellington, S. M. Aschmann, J. Arey, A. M. Winer and J. N. Pitts, Atmospheric Chemistry of Aniline, N,N-Dimethylanillne, Pyridine, 1,3,5-Triazine, and Nitrobenzene, *Environ. Sci. Technol.*, 1987, **21**, 64–72.

13 T. B. Brill and K. J. James, Kinetics and Mechanisms of Thermal Decomposition of Nitroaromatic Explosives, *Chem. Rev.*, 1993, **93**, 2667–2692.

14 H. Nakagawa, K. Hishikawa, K. Eto, N. Ieda, T. Namikawa, K. Kamada, T. Suzuki, N. Miyata and J. I. Nabekura, Fine spatiotemporal control of nitric oxide release by infrared pulse-laser irradiation of a photolabile donor, *ACS Chem. Biol.*, 2013, **8**, 2493–2500.

15 J. S. Zugazagoitia, C. X. Almora-Díaz and J. Peon, Ultrafast intersystem crossing in 1-nitronaphthalene. An experimental and computational study, *J. Phys. Chem. A*, 2008, **112**, 358–365.

16 Y. Orozco-Gonzalez, K. Coutinho, J. Peon and S. Canuto, Theoretical study of the absorption and nonradiative deactivation of 1-nitronaphthalene in the low-lying singlet and triplet excited states including methanol and ethanol solvent effects, *J. Chem. Phys.*, 2012, **137**, 54307.

17 A. Giussani, Toward the understanding of the photophysics and photochemistry of 1-nitronaphthalene under solar radiation: The first theoretical evidence of a photodegradation intramolecular rearrangement mechanism involving the triplet states, *J. Chem. Theory Comput.*, 2014, **10**, 3987–3995.

18 A. A. Granovsky, Extended multi-configuration quasi-degenerate perturbation theory: The new approach to multi-state multi-reference perturbation theory, *J. Chem. Phys.*, 2011, **134**, 1–14.

19 I. Fdez. Galván, M. Vacher, A. Alavi, C. Angeli, F. Aquilante, J. Autschbach, J. J. Bao, S. I. Bokarev, N. A. Bogdanov, R. K. Carlson, L. F. Chibotaru, J. Creutzberg, N. Dattani, M. G. Delcey, S. S. Dong, A. Dreuw, L. Freitag, L. M. Frutos, L. Gagliardi, F. Gendron, A. Giussani, L. González, G. Grell, M. Guo, C. E. Hoyer, M. Johansson, S. Keller, S. Knecht, G. Kovačević, E. Källman, G. Li Manni, M. Lundberg, Y. Ma, S. Mai, J. P. Malhado, P. Å. Malmqvist, P. Marquetand, S. A. Mewes, J. Norell, M. Olivucci, M. Oppel, Q. M. Phung, K. Pierloot, F. Plasser, M. Reiher, A. M. Sand, I. Schapiro, P. Sharma, C. J. Stein, L. K. Sørensen, D. G. Truhlar, M. Ugandi, L. Ungur, A. Valentini, S. Vancoillie, V. Veryazov, O. Weser, T. A. Wesołowski, P. O. Widmark, S. Wouters, A. Zech, J. P. Zobel and R. Lindh, OpenMolcas: From Source Code to Insight, *J. Chem. Theory Comput.*, 2019, **15**, 5925–5964.

20 G. Li Manni, I. Fdez. Galván, A. Alavi, F. Aleotti, F. Aquilante, J. Autschbach, D. Avagliano, A. Baiardi, J. J. Bao, S. Battaglia, L. Birnoschi, A. Blanco-González, S. I. Bokarev, R. Broer, R. Cacciari, P. B. Calio, R. K. Carlson, R. Carvalho Couto, L. Cerdán, L. F. Chibotaru, N. F. Chilton, J. R. Church, I. Conti, S. Coriani, J. Cuéllar-Zuquin, R. E. Daoud, N. Dattani, P. Decleva, C. de Graaf, M. G. Delcey, L. De Vico, W. Dobrautz, S. S. Dong, R. Feng, N. Ferré, M. Filatov(Gulak), L. Gagliardi, M. Garavelli, L. González, Y. Guan, M. Guo, M. R. Hennefarth, M. R. Hermes, C. E. Hoyer, M. Huix-Rotllant, V. K. Jaiswal, A. Kaiser, D. S. Kaliakin, M. Khamesian, D. S. King, V. Kochetov, M. Krośnicki, A. A. Kumaar, E. D.

Larsson, S. Lehtola, M. B. Lepetit, H. Lischka, P. López Ríos, M. Lundberg, D. Ma, S. Mai, P. Marquetand, I. C. D. Merritt, F. Montorsi, M. Mörchen, A. Nenov, V. H. A. Nguyen, Y. Nishimoto, M. S. Oakley, M. Olivucci, M. Oppel, D. Padula, R. Pandharkar, Q. M. Phung, F. Plasser, G. Raggi, E. Rebolini, M. Reiher, I. Rivalta, D. Roca-Sanjuán, T. Romig, A. A. Safari, A. Sánchez-Mansilla, A. M. Sand, I. Schapiro, T. R. Scott, J. Segarra-Martí, F. Segatta, D. C. Sergentu, P. Sharma, R. Shepard, Y. Shu, J. K. Staab, T. P. Straatsma, L. K. Sørensen, B. N. C. Tenorio, D. G. Truhlar, L. Ungur, M. Vacher, V. Veryazov, T. A. Voß, O. Weser, D. Wu, X. Yang, D. Yarkony, C. Zhou, J. P. Zobel and R. Lindh, The OpenMolcas Web: A Community-Driven Approach to Advancing Computational Chemistry, *J. Chem. Theory Comput.*, , DOI:10.1021/acs.jctc.3c00182.

21 P. O. Widmark, P. Å. Malmqvist and B. O. Roos, Density matrix averaged atomic natural orbital (ANO) basis sets for correlated molecular wave functions - I. First row atoms, *Theor. Chim. Acta*, 1990, **77**, 291–306.

22 K. Pierloot, B. Dumez, P.-O. Widmark and B. O. Roos, Density matrix averaged atomic natural orbital (ANO) basis sets for correlated molecular wave functions, *Theor. Chim. Acta*, 1995, **90**, 87.

23 B. Szefczyk, D. Grabarek, E. Walczak and T. Andruniow, Excited-State Minima and Emission Energies of Retinal Chromophore Analogues : Performance of CASSCF and CC2 Methods as Compared with CASPT2 w, 2017, **38**, 1799–1810.